

Synchronized delivery of Er:YAG-laser-pulse energy during oscillations of vapor bubbles

Peter Gregorcic¹, Marko Jamsek¹, Matjaz Lukac², Matija Jezersek¹

¹Faculty of Mechanical Engineering, University of Ljubljana, Ljubljana, Slovenia

²Fotona, d.d., Ljubljana, Slovenia

ABSTRACT

A laser system and a measuring method for the synchronized delivery of multiple Er:YAG-laser pulses during vapor-bubble oscillations are presented. We use a free-running Er:YAG laser, designed for laser dentistry. Our results reveal that for short Er:YAG laser pulses, spherical bubbles develop even if a flat-end fiber tip is used for delivery of the Er:YAG-laser pulses into water.

We developed a method called a laser-beam-transmission probe for on-line monitoring of the bubbles' oscillations. By using this method combined with shadowgraphy, we show that the dissipation of the bubbles' energy during bubble oscillations can be efficiently balanced by the synchronized delivery of multiple Er:YAG-laser pulses. Our results show that the resonance effect is obtained when the second laser pulse is delivered at the end or slightly after the bubble's collapse. In this case the resonance effect increases the mechanical energy of the secondary oscillations. The presented PHAST (Photo Acoustic Synchronized Transients) method has great potential to open new opportunities for further development of modern laser-based dental treatments.

Key words: Er:YAG, multiple pulses, vapor bubble, shadow photography, laser-beam-transmission probe, laser dentistry, endodontics, resonance effect, PHAST optodynamics

Article: J. LA&HA, Vol. 2014, No.1; pp.14-19.

Received: July 9, 2014; Accepted: July 22, 2014

© Laser and Health Academy. All rights reserved.
Printed in Europe. www.laserandhealth.com

I. INTRODUCTION

Effective irrigation, including debriding, cleaning and decontamination of the anatomical cavities, is one of the most important challenges in different areas of dentistry, such as endodontics, implantology, periodontics, or bone surgery [1]. For example, one of the main goals in nonsurgical endodontic treatment is an efficient cleaning and decontamination of the smear layer, bacteria and their byproducts within the root canal [2, 3].

Conventional endodontic techniques use mechanical instrumentation as well as ultrasonic and chemical irrigation to debride and remove the infective microorganisms from the endodontic system [4]. Since these conventional techniques are not able to completely decontaminate the complex root canal anatomy [5], medium-infrared lasers have been introduced as an improvement of conventional cleaning [6-9].

Recent studies [2-4, 10] have proven that the usage of a free-running erbium (Er:YAG) laser that radiates low-energy (20-60 mJ) pulses with duration of 50 µs is a very promising technique for endodontic treatment of the root canal. In these procedures, the Er:YAG pulses are delivered into the pulpal chamber using fiber tips (FTs) with different geometries. Among all the infrared lasers, the Er:YAG laser, emitting pulsed light at 2.94 µm, has the highest absorption in water [11]. Due to its very high absorption coefficient ($\mu_a = 1.247 \times 10^6 \text{ m}^{-1}$) more than 70% of all the pulse light is absorbed within a water layer only 1 µm thick. Thus, the water is locally and instantly heated over the boiling point and a vapor bubble starts to form at the FT's end [7, 12, 13].

After the explosive boiling, the vapor bubble starts to expand. When it reaches its maximum volume, it is nearly empty and starts to collapse due to the pressure of the surrounding liquid. This collapse, in turn, initiates the secondary bubble's growth and collapse. The process repeats itself, resulting in so-called vapor-bubble oscillations. Here, each oscillation has less energy and therefore reaches smaller volume due to energy dissipation during each oscillation [13, 14].

In our previous study [13] we have shown that in the case of the conical FT, a spherical bubble is induced, while a channel-like bubble develops for the flat-end FT. Moreover, in the same study we had also shown that the optodynamic (OD) efficiency, defined as the ratio between the mechanical energy of the liquid medium and the pulse energy, increases with decreasing pulse duration. Therefore, the first aim of this paper is to study the sub-microsecond Er:YAG laser pulses at ultra-low-energy (less than 2 mJ). According to our previous results [13], these pulses have the potential to significantly increase the OD

efficiency. A method called a laser-beam-transmission probe (LBTP) for on-line monitoring of the bubble's oscillations [15] was developed to carry out the study.

The second goal of this paper is to show that the dissipation of the bubble's energy during bubble oscillations can be efficiently enhanced by a synchronized delivery of the Er:YAG-laser-pulse energy at the end of the vapor-bubble collapse. This method, called Photo Acoustic Synchronized Transients (PHAST), promises to further improve upon the safety and efficacy of modern laser endodontics.

II. EXPERIMENTAL SETUP

There are three main components of the experimental setup, schematically shown in Fig. 1: (i) the excitation source, where we have used a free-running Er:YAG laser, designed for laser dentistry; and two measuring methods that were simultaneously employed for the monitoring of the vapor bubble dynamics: (ii) high-speed shadowgraphy, and (iii) LBTP. All three modules of our experimental setup are described in detail in the following subsections.

The experimental setup is automatically controlled with a personal computer (PC) by using custom-developed software that also enables setting the excitation-laser parameters, the data acquisition from a digital oscilloscope, image acquisition as well as data and image processing.

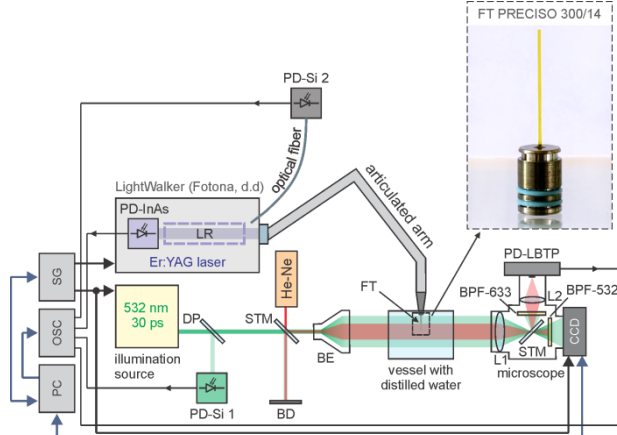


Fig. 1: Schematic view of the experimental setup.

a) An excitation system

We used a free-running Er:YAG laser, designed for laser dentistry ($\lambda = 2.940 \mu\text{m}$, Fotona, d.d., Slovenia, LightWalker). The flash-lamp power as a function of time was monitored by using a 10-MHz Si photodiode (PD-Si 2), where the light from the flash lamp to the PD-Si 2 was guided through an optical fiber, as schematically shown in Fig. 1. The Er:YAG-pulse

power as a function of time was measured by a 60-MHz InAs photodiode (PD-InAs) placed behind the rear mirror of the laser resonator (LR). The signals from photodiodes were acquired by a digital oscilloscope (OSC; LeCroy, US, 600 MHz Wave Runner 64MXi-A).

The Er:YAG laser was operated to radiate one or two single pulses with peak powers of around 900 W and FWHM less than 1 μs , which followed one another at an adjustable temporal separation in the range of 130 - 170 μs (e.g., see the blue curves in Figs. 3-6).

The delivery of the laser pulses into the vessel with distilled water was performed through an articulated arm. Within the handpiece, the pulse was optically coupled into an interchangeable FT. For our experiments we used a Fotona Preciso 300/14 fiber tip, shown in the inset of Fig. 1. Here, the FT was 14 mm long and had a flat end with a diameter of 300 μm .

b) Laser-based shadowgraphy

To observe the spatial distribution of the optodynamic phenomena induced by Er:YAG laser in a liquid [13, 14, 16, 17], we employed laser-based shadowgraphy [13]. Laser shadowgraphy enables two-dimensional spatial observations, but only in a single time instance [16]. Thus, multiple events should be captured at different delays between the excitation and illumination pulse to acquire the vapor-bubble dynamics.

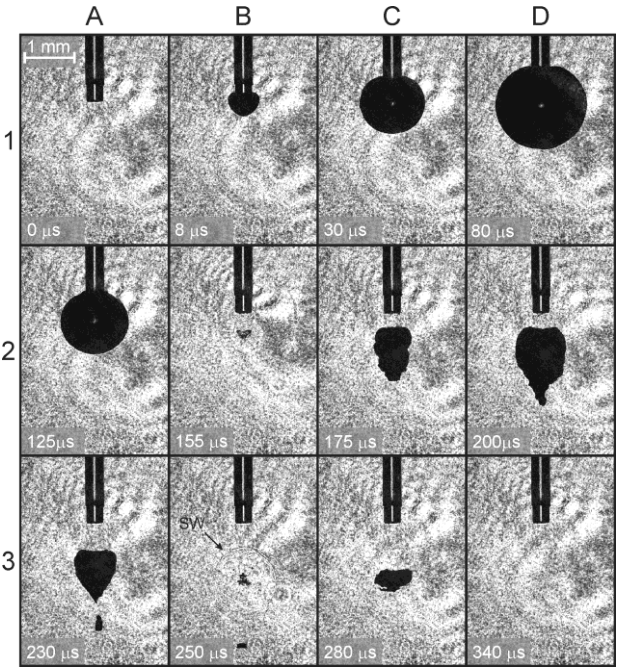


Fig. 2: Typical series of shadowgraphs for a single Er:YAG-laser pulse with pulse duration (FWHM) of $0.7 \mu\text{s} \pm 0.2 \mu\text{s}$ and pulse energy of $2.0 \text{ mJ} \pm 0.2 \text{ mJ}$. The scale is shown on the top-left-hand side of the first image, while the time after the excitation pulse is shown on the bottom-left-hand side of each image.

The main idea of the shadowgraphy is to use a short illumination pulse (pulsed probe) and a CCD camera. Thus, a frequency-doubled Nd:YAG laser (Ekspla, Lithuania, PL2250-SH-TH) emitting green ($\lambda = 532$ nm) pulses with duration of 30 ps was used as the pulsed probe. To determine the accurate time of the illumination, the probe was partially reflected by a dielectric plate (DP) to the 1-GHz Si-photodiode (PD-Si 1) as shown in Fig. 1. A beam expander (BE) was placed in front of the laser-pulse – water interaction area. The image was captured throughout a microscope equipped with a charged-coupled device (CCD) camera (Basler AG, Germany, scA1400-17fm, 1.4 Mpx). A narrow band-pass filter (BPF-532; 532 nm \pm 10 nm) was placed in front of the CCD to block the light from the He-Ne laser, used for LBTP. The spatial resolution of our optical system during the measurements was $\kappa = 4.2$ mm/pixel. It was determined using the images of a calibrated pattern.

The excitation laser, illumination laser and camera were synchronized with the SG connected to the PC. Here, each image was captured at a different delay between the excitation and illumination pulses. This delay was set by the SG.

A typical series of shadowgraphs for a single Er:YAG-laser pulse with pulse duration (FWHM) of $0.8 \text{ ns} \pm 0.2 \mu\text{s}$ and pulse energy of $2.0 \text{ mJ} \pm 0.2 \text{ mJ}$ (see the blue curve in Fig. 3) is shown in Fig. 2. Here, the image occurs due to local changes of the refractive index in a medium that deflects the path of the probe beam casting a shadow [18]. Since the FT and the vapor bubble locally change the refractive index, they are both visible as a dark area on the bright background due to the deflection of the pulsed probe on the refractive index gradient. Before the radiation of the Er:YAG pulse, only the FT appears on the image, as visible from A1 in Fig. 2.

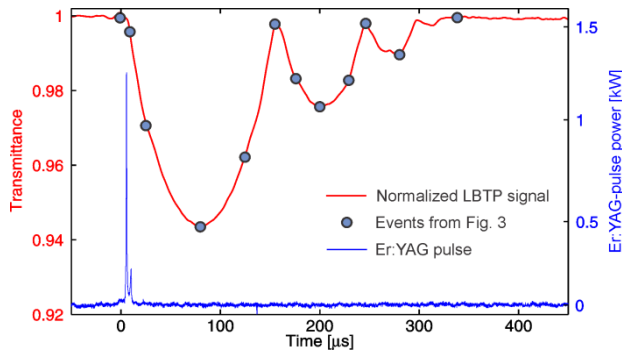


Fig. 3: The normalized transmittance of a typical LBTP signal (the left-hand-side axis and the red curve) for a single Er:YAG-laser pulse (the right-hand-side axis and the blue curve). The blue circles show the events from Fig. 3.

c) Laser-beam-transmission probe

To observe the whole bubble's dynamics from a single Er:YAG-laser shot, we simultaneously employed another method, called a laser-beam-transmission probe (LBTP). The main idea of this method is very similar to the idea of the shadowgraphy, described above. As with shadowgraphy, LBTP also detects the local changes of the refractive index within the probe-beam's path. However, the main difference is that shadowgraphy is able to detect the 2D spatial distribution of the bubble, but only in a single time instance. Therefore *multiple events* are necessary to capture the bubble's dynamics, as presented in Fig. 2. On the other hand, LBTP is able to detect the whole bubble's dynamics from a *single* shot, but cannot detect its spatial distribution.

In the case of LBTP the continuous-wave (CW) illumination probe is needed. For this reason we employed a He-Ne laser as the CW probe for LBTP, as shown in Fig. 1. This CW probe was coupled into the same path as the pulsed probe for the shadowgraphy using a semi-transparent mirror (STM). After this coupling, the CW probe was led through the same BE as a pulsed probe and it illuminated the same laser-pulse – water-interaction area as the pulsed probe for shadowgraphy.

Another semi-transparent mirror (STM) was used inside the microscope to deflect the CW probe into the lens (L2). A narrow band-pass filter (BPF-633; 532 nm \pm 10 nm) was placed in front of L2 to block the green pulsed probe of the shadowgraphic method. Lens L2 collects all transmitted CW-probe light into the 150-MHz Si photodiode (PD-LBTP).

The red curve in Fig. 3 shows a typical LBTP signal for the same bubble, as presented in Fig. 2. The single events A1-D3 from Fig. 2 are marked by the blue circles in Fig. 3. The right-hand-side axis shows the power of the Er:YAG-laser pulse (the blue curve), while the left-hand-side axis shows the normalized transmittance of the LBTP signal (the red curve).

Since lens L2 collects all of the CW-probe light on a *single* photodetector, the LBTP technique measures the transmittance of the CW probe. In analogy, its signal at any time t is proportional to the sum of the pixels' values in the shadowgraph image captured at the same time t . Thus, before the Er:YAG pulse, the CW probe is blocked only by a FT, as is visible from image A1 in Fig. 2. Consequently, at these times the LBTP signal reaches its maximum value (e.g., the first blue circle in Fig. 3 that corresponds to image A1 in Fig. 2). When bubble starts to develop, less of

the CW probe is transmitted through the interaction area and the LBTP signal starts to decrease (e.g., compare the second blue point in Fig. 3 and the image B1 in Fig. 3). When the vapor bubble reaches its maximum value, the LBTP signal reaches its minimum value. In our case this happens 80 μ s after the Er:YAG pulse (image D1 in Fig. 2 and the fourth blue point in Fig. 3). Then the bubble starts to collapse (e.g., images A2 and B2 in Fig. 2) and the LBTP signal starts to increase (e.g., the fifth and the sixth blue point in Fig. 3). After the collapse, the bubble oscillations repeat several times, as is also clearly visible from the LBTP signal.

III. RESULTS

a) Bubble's Dynamics

The bubble's dynamics for a single Er:YAG-laser pulse (FWHM of 0.8 μ s \pm 0.2 μ s and pulse energy of 2.0 mJ \pm 0.2 mJ; see the blue curve in Fig. 3) is presented in Figs. 2 and 4. The results of our previous work [13] show that a channel-like bubble is formed when an Er:YAG pulse of duration longer than 40 μ s is delivered into water through a 300 μ m flat-end FT. However, a typical series of shadowgraph images in Fig. 2 reveal that near-microsecond pulses induce a spherical bubble also in the case of the flat-end FT. This finding is in accordance with the results obtained by Jansen et al. [19], who compared the bubbles induced by a Ho:YAG laser in water.

When the vapor bubble reaches its maximum volume (e.g., see image D1 in Fig. 2) it is nearly empty [20] and starts to collapse due to the pressure of the surrounding liquid. As is clearly seen from image A2 in Fig. 2, the vapor bubble keeps its spherical shape during the first collapse. At the end of the collapse, the bubble almost disappears (see image B2 in Fig. 2) and the LBTD transmittance reaches values near 1, as is visible from the sixth blue point in Fig. 3.

During the second oscillation the bubble becomes elongated, as is visible from images C2-A3 in Fig. 2. After the collapse a shock wave is emitted (SW in image B3 in Fig. 2).

Comparison of shadowgraph images in Fig. 2 with the LBDP signal in Fig. 3 shows that the bubble's volume is inversely proportional to the LBTP transmittance. Thus, a smaller transmittance means larger bubble volume. Since the bubble's volume is proportional to the mechanical energy of the liquid medium [14], it can be conclude that lower LBTP transmittance means larger mechanical energy.

In Fig. 3, three bubbles' oscillations are visible.

Here, each oscillation has less mechanical energy due to energy dissipation. This is in accordance with the findings of other authors [21].

b) Synchronized delivery of Er:YAG-pulse energy

It is well known that the vapor bubble loses its energy during oscillations. To balance this dissipation of the bubble's energy, we used two Er:YAG-laser pulses delayed by 130-170 μ s, as shown by the blue curve in Figs. 5-7. Here, the first pulse has energy of 2.0 mJ \pm 0.2 mJ, and FWHM of 0.8 μ s \pm 0.2 μ s, while the energy of the second pulse was 2.2 mJ \pm 0.2 mJ and its FWHM was 0.7 μ s \pm 0.2 μ s. For a better comparison of the results, the vapor bubble, induced by a single pulse (from Fig. 3) is shown by a gray dashed line in Figs. 5-7 as a reference LBTP signal.

The red curve in Fig. 4 shows the vapor bubble's oscillations, if the second Er:YAG pulse is radiated 150 μ s later than the first Er:YAG pulse, i.e., exactly at the end of the first bubble's collapse. In this case, the synchronized delivery of additional Er:YAG energy increases the mechanical energy of the liquid medium. Consequently, the volume of the second bubble significantly increases due to the resonance effect, as is visible from the comparison between the normalized (the red curve) and the reference (the gray dashed curve) LBTP signal in Fig. 4. Moreover, in this case the mechanical energy of the second oscillation is even larger than the mechanical energy of the first bubble's oscillation and the number of the oscillations increases from three (e.g., see the dashed curve) to four (e.g., see the red curve).

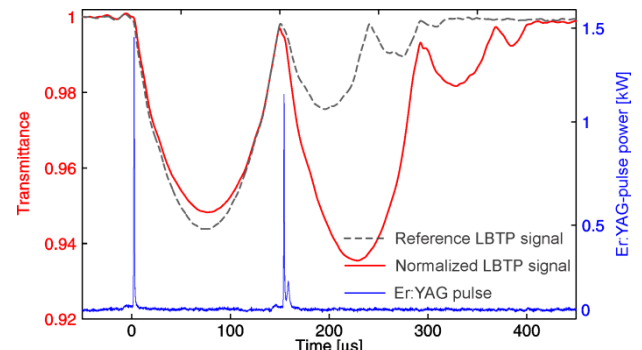


Fig. 4: Typical LBTP signal (the left-hand-side axis and the red curve) for double Er:YAG-laser pulses (the right-hand-side axis and the blue curve). The second Er:YAG pulse was radiated 150 μ s after the first pulse, i.e., exactly at the end of the first bubble's collapse. The reference signal (LBTP signal from Fig. 3) is shown by the gray dashed line.

The importance of the synchronized delivery of multiple Er:YAG-laser pulses during the bubble's oscillations is clearly visible from Fig. 5. The red curve in Fig. 5 shows the bubble's oscillations when the second Er:YAG pulse is delivered before the end of

the bubble's first oscillation. In this case the resonance effect is not obtained and the mechanical energy of the second and the third oscillation is not increased.

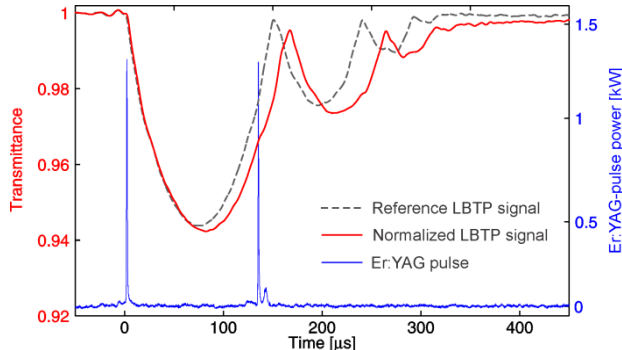


Fig. 5: Typical LBTP signal (the left-hand-side axis and the red curve) for double Er:YAG-laser pulses (the right-hand-side axis and the blue curve). The second Er:YAG pulse was radiated 130 μ s later than the first pulse, i.e., before the end of the first bubble's collapse. The reference signal (LBTP signal from Fig. 3) is shown by the gray dashed line.

Figure 6 shows the LBTP signal (the red curve), when the first and the second Er:YAG pulses are delayed by 170 μ s (e.g., see the blue curve). In this case, the second pulse is delivered after the first bubble's collapse. Here, we can also observe a similar effect as in the case of Fig. 4.

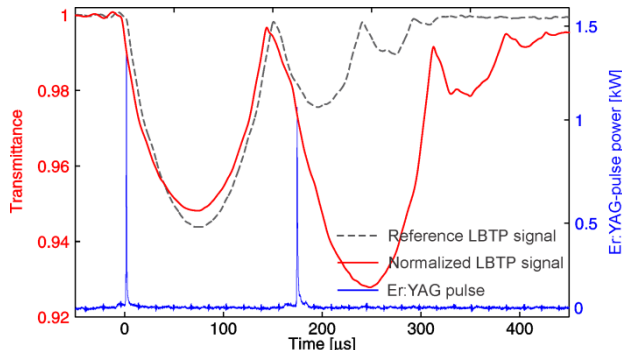


Fig. 6: Typical LBTP signal (the left-hand-side axis and the red curve) for double Er:YAG-laser pulses (the right-hand-side axis and the blue curve). The second Er:YAG pulse was radiated 170 μ s after the first pulse, i.e., after the end of the first bubble's collapse. The reference signal (LBTP signal from Fig. 3) is shown by the gray dashed line.

IV. DISCUSSION

Two Er:YAG pulses have approximately twice the larger energy of a single Er:YAG pulse. Thus, if they do not increase the mechanical energy of the liquid medium in comparison with a single Er:YAG-pulse radiation, the OD efficiency [13] is significantly decreased. From Figs. 4, 5 and 6 it can therefore be concluded that in the case of multiple Er:YAG pulses, it is important to not deliver the second pulse before

the end of the bubble's first oscillation. Instead, the second Er:YAG-laser pulse should be delivered at the end or slightly after the bubble's collapse. In such cases a PHAST resonance effect is obtained which increases the mechanical energy of the secondary bubble's oscillations.

The prolonged PHAST oscillations are expected to lead to additional clinical benefits, in addition to the enhanced opto-acoustic energy conversion efficiency. For example, it is well known that when bacteria are submitted to increased temperatures, the kill rate depends not only on the amplitude of the temperature increase, but even more importantly, on the temporal duration of the temperature increase, the exact dependence being described by the standard Arrhenius integral [22]. Similar consideration applies also when bacteria are submitted to acoustic transients. When subjected to acoustic transients, the bacteria's structure is disrupted and the bacteria die, providing that the exposure to the transients is extensive enough to be fatal. The bacterial kill rate is thus expected to be much higher when bacteria are submitted to the PHAST oscillations for a longer duration of time.

V. CONCLUSIONS

By using a new laser-beam-transmission probe technique, we measured the bubble dynamics and the resonance effect induced by the delivery of multiple laser pulses during bubble oscillations. Our results reveal that for short Er:YAG laser pulses, spherical bubbles develop even if a flat-end fiber tip is used for delivery of the Er:YAG-laser pulses into water.

We have also shown that in the case of the delivery of multiple laser pulses, the resonance effect is obtained when the second pulse is delivered at the end of or slightly after the bubble's first collapse. In this case the resonance effect increases the mechanical energy of the secondary oscillations. On the other hand, if the second pulse is delivered before the end of the bubble's first oscillation, it decreases the optodynamic energy-conversion efficiency and therefore decreases the efficiency of the laser treatment.

The presented PHAST laser method for synchronized delivery of Er:YAG-laser pulses during bubble oscillations has great potential for different medical applications in laser dentistry. We believe that these results will open new opportunities for further development of modern laser-based dental treatments.

ACKNOWLEDGMENT

This study was financed by the European Fund for Regional Development, the Slovenian Ministry of Education, Science, Culture and Sport, and by Fotona, d.d. We would like to thank Fotona, d.d for supplying their commercially available laser system for laser cleaning of root canals in clinical dental applications. Their system, including the Er:YAG laser (LightWalker), handpiece and interchangeable fiber tips, was used as an excitation source in our experiments.

REFERENCES

1. Lukac M, Pustovrh G. Modeling Photoacoustic Efficiency during Erbium Laser Endodontics. *Journal of the Laser and Health Academy*. 2013 Dec; 2013(2):1-5.
2. Olivi G, DiVito E. M Photoacoustic Endodontics using PIPSTM: experimental background and clinical protocol. *Journal of the Laser and Health Academy*. 2012 May; 2012(1):22-25.
3. DiVito E, Peters OA, Olivi G. Effectiveness of the erbium:YAG laser and new design radial and stripped tips in removing the smear layer after root canal instrumentation. *Laser Med Sci* 2012 Apr;27(2):273-280.
4. Peters OA, Bardsley S, Fong J, Pandher G, DiVito E. Disinfection of Root Canals with Photon-initiated Photoacoustic Streaming. *J Endodont* 2011 Jul;37(7):1008-1012.
5. Huang TY, Gulabivala K, Ng YL. A bio-molecular film ex-vivo model to evaluate the influence of canal dimensions and irrigation variables on the efficacy of irrigation. *Int Endod J* 2008 Jan;41(1):60-71.
6. Takeda FH, Harashima T, Kimura Y, Matsumoto K. Efficacy of Er:YAG laser irradiation in removing debris and smear layer on root canal walls. *J Endodont* 1998 Aug;24(8):548-551.
7. Matsumoto H, Yoshimine Y, Akamine A. Visualization of Irrigant Flow and Cavitation Induced by Er:YAG Laser within a Root Canal Model. *J Endodont* 2011 Jun;37(6):839-843.
8. Glover DL, DiVito EE, Tubbs KA, Colonna MP. Laser based enhanced generation of photoacoustic pressure waves in dental and medical treatments and procedures. United States Patent US 7,959,441 B2 2011 Jun.
9. Licata ME, Albanese A, Campisi G, Geraci DM, Russo R, Gallina G. Effectiveness of a new method of disinfecting the root canal, using Er, Cr:YSGG laser to kill Enterococcus faecalis in an infected tooth model. *Laser Med Sci* 2013 Aug [In Press].
10. Deleu E, Meire M, Moor RG. Efficacy of laser-based irrigant activation methods in removing debris from simulated root canal irregularities. *Laser Med Sci* 2013 Oct; [In Press].
11. Hale GM, Querry MR. Optical-Constants of Water in 200-Nm to 200-Mum Wavelength Region. *Appl Optics* 1973 Aug;12(3): 555-563.
12. Vogel A, Venugopalan V. Mechanisms of pulsed laser ablation of biological tissues. *Chem Rev* 2003 Feb;103(2):577-644.
13. Gregorcic P, Jezersek M, Mozina J. Optodynamic energy-conversion efficiency during an Er:YAG-laser-pulse delivery into a liquid through different fiber-tip geometries. *J Biomed Opt* 2012 Jul;17(7):075006.
14. Petkovsek R, Gregorcic P. A laser probe measurement of cavitation bubble dynamics improved by shock wave detection and compared to shadow photography. *J Appl Phys* 2007 Aug, 102(4):044909.
15. Devia-Cruz Luis F, Camacho-López S, Evans R, García-Casillas D, Stepanov S. Laser-induced cavitation phenomenon studied using three different optically-based approaches – An initial overview of results. *Photonics and Lasers in Medicine* 2012 Aug;1(3):195-205.
16. Gregorcic P, Petkovsek R, Mozina J, Mocnik G. Measurements of cavitation bubble dynamics based on a beam-deflection probe. *Appl Phys A* 2008 Dec;93(4):901-905.
17. Petkovsek R, Gregorcic P, Mozina J. A beam-deflection probe as a method for optodynamic measurements of cavitation bubble oscillations. *Meas Sci Technol* 2007 Sep;18(9):2972-2978.
18. Settles GS (2001) Schlieren and Shadowgraph Techniques: visualizing phenomena in transparent media. Springer-Verlag, Berlin.
19. Jansen ED, Asshauer T, Frenz M, Motamedi M, Delacretaz G, Welch AJ: Effect of pulse duration on bubble formation and laser-induced pressure waves during holmium laser ablation. *Laser Surg Med* 1996;18(3):278-293.
20. Vogel A (2001) Optical Breakdown in Water and Ocular Media, and its Use for Intraocular Photodisruption. Shaker Verlag GmbH, Aachen.
21. Vogel A, Lauterborn W, Timm R. Optical and Acoustic Investigations of the Dynamics of Laser-Produced Cavitation Bubbles near a Solid Boundary. *J Fluid Mech* 1989 Sep;206:299-338.
22. Simanovskii D.M., Mackanos M.A., Irani A.R., O'Connell-Rodwell C.E., Contag C.H., Schwettman H.A., Palanker D.V. Cellular tolerance to pulsed hyperthermia. *Phys Rev E* 74, 2006; 011915: 1-7.

The intent of this Laser and Health Academy publication is to facilitate an exchange of information on the views, research results, and clinical experiences within the medical laser community. The contents of this publication are the sole responsibility of the authors and may not in any circumstances be regarded as official product information by medical equipment manufacturers. When in doubt, please check with the manufacturers about whether a specific product or application has been approved or cleared to be marketed and sold in your country.